Pt_2Tl Building Blocks for 2D Extended Solids: Synthesis, Crystal Structures and Luminescence

Sara Fuertes,[a] Andrés J. Chueca,[a] Antonio Martín,[a] and Violeta Sicilia[b]*

[a] Departamento de Química Inorgánica, Facultad de Ciencias, Instituto de Síntesis Química y Catálisis Homogénea (ISQCH), CSIC - Universidad de Zaragoza, Pedro Cerbuna 12, 50009, Zaragoza (Spain)

[b] Departamento de Química Inorgánica, Escuela de Ingeniería y Arquitectura de Zaragoza, Instituto de Síntesis Química y Catálisis Homogénea (ISQCH), CSIC - Universidad de Zaragoza, Campus Río Ebro, Edificio Torres Quevedo, 50018, Zaragoza (Spain).E-mail: sicilia@unizar.es

ABSTRACT

The *β*-diketonate compounds of Pt(II), [Pt(R-C^C*)(acac)] (acacH = acetylacetone, R-CH^C* = 1-(4-cyanophenyl)-3-methyl-1*H*-imidazol-2-ylidene (NC-CH^C*) **1A**, 1-(4-(ethoxycarbonyl)phenyl)-3-methyl-1*H*-imidazol-2-ylidene (CO_2Et-CH^C*) **1B**, 1-(3,5-dichlorophenyl)-3-methyl-1*H*-imidazol-2-ylidene (Cl-CH^C*) **1C**) containing cyclometalated N-heterocyclic carbenes were synthesized from compounds [{Pt(μ-Cl)(R-C^C*)}$_2$] (R = CN **A**, CO_2Et **B**, Cl **C**). Compound **C** was prepared for the first time following the step by step protocol used to synthesize **A** and **B**. The X-ray structures of complexes **1B** and **1C** show that only in **1B** the molecules stack in pairs through intermolecular Pt···Pt (3.370 Å) and π - π (~ 3.43 Å) interactions between the NHC ligand and the acac. The reaction of compounds **1A**–**1C** with $TlPF_6$ (2:1 molar ratio) leads to the

clusters [{Pt(R-C^C*)(acac)}$_2$Tl]$^+$ (R = CN **2A**, CO_2Et **2B**, Cl **2C**), which exhibit a "Pt_2Tl" sandwich structure, where two slightly distorted square planar "Pt(R-C^C*)(acac)" subunits are bonded to a Tl(I) center through donor-acceptor Pt-Tl bonds. Compounds **2A** and **2B** show an extended 2D lattice in the solid state through intermolecular Pt··Pt and Tl-E (E = N, O) interactions, meanwhile **2C** forms discrete molecules without any kind of intermolecular interaction among them. The effects of the R substituent and the Pt-Tl interactions on the crystal structures and the photophysical properties have been investigated.

INTRODUCTION

The Lewis basic properties of transition metals play an important role for catalytic cycles[1-3] and also lead to metal clusters through the formation of metal–metal dative bonds.[4-9] The high electron density of Pt (II) in square-planar complexes has been demonstrated many times by their role as the Lewis base unit in unsupported metal-only Lewis pair (MOLP) compounds. Among Pt(II) → M (M = Cu^I, Ag^I, Au^I, Cd^{II}, Hg^{II}, Tl^I, Sn^{II}, Pb^{II}) MOLP complexes,[5, 9] the silver-containing ones are still the most numerous,[5] but examples of Pt(II) (d^8) → Tl(I) ($d^{10}s^2$) clusters[10-11] are increasing since A. L. Balch published [$Tl_2Pt(CN)_4$], the first blue-luminescent columnar compound containing Pt-Tl bonds.[12] In this field have been reported luminescent Pt^{II}-Tl^I MOLP clusters showing diverse structural configurations, including dinuclear (PtTl),[13-15] trinuclear (Pt_2Tl,[10, 16] $PtTl_2$[12, 17-19]), tetranuclear (Pt_3Tl, $(PtTl)_2$),[13, 19-20] hexanuclear clusters (Pt_2Tl_4, Pt_3Tl_3),[20-22] or infinite networks,[10-11, 16, 21, 23] many of them containing C,N-cycloplatinated compounds as Lewis base unit.[10, 13, 15, 20] In many cases their luminescent properties have been demonstrated to depend on the Pt-Tl interactions.[10, 12-21] Moreover, the formation of the metal-metal bond

affects the crystal packing allowing or hindering the molecular assembly through π-π interactions, with the subsequent effect on the emitting properties.[11, 13]

The use of N-heterocyclic carbenes (NHCs) as cyclometalated ligands has been revealed as a key to get stable and very efficient Pt(II) phosphorescent emitters.[24-27] Compared to C,N-cycloplatinated compounds, the even greater heightening of the d-d energy levels on the metal center, enlarging the energy gap with the emissive excited states, avoids the thermal quenching and improves the emission quantum yields. Examples of phosphorescent compounds of platinum(II) containing C^C*-cyclometalated NHCs ligands are still fairly limited and the effect of metallophilic interactions on the emission properties have been barely investigated.[28] Because of that our task in this work was to prepare unsupported Pt^{II}-Tl^{I} MOLP structures, containing cyclometalated N-heterocyclic carbene complexes of Pt(II) as Lewis base units to gauge for the first time the ability of this kind of Pt(II) complexes to act as Lewis bases for this kind of interactions, the stability of these interactions and the effect of them in the photophysical properties of the mononuclear Pt(II) complexes.

With this purpose we prepared the *β*-diketonate compounds [Pt(R-C^C*)(acac)] (acacH = acetylacetone, R-CH^C* = 1-(4-cyanophenyl)-3-methyl-1*H*-imidazol-2-ylidene (CN-CH^C*) **1A**, 1-(4-(ethoxycarbonyl)phenyl)-3-methyl-1*H*-imidazol-2-ylidene (CO_2Et-CH^C*) **1B**, 1-(3,5-dichlorophenyl)-3-methyl-1*H*-imidazol-2-ylidene (Cl-CH^C*) **1C**) and the Pt_2Tl clusters derived from them. In this way we have been able to compare first the effect of the R-C^C group on the luminescent properties of the mononuclear Pt(II) complexes and in their ability to form Pt_2Tl clusters. The luminescence of these mononuclear compounds has been explained considering the TD- DFT calculations and X-ray diffraction studies.

The synthesis of **1A–1C** was carried out using compounds [{Pt(μ-Cl)(C^C*)}$_2$] (CN-C^C* **A**, CO_2Et-C^C* **B**, Cl-C^C* **C**) as starting materials, like in a previous work.[26] Compound **C** was prepared for the first time following our stepwise protocol for this kind of complexes and has been fully described in the Supporting Information.

EXPERIMENTAL SECTION.

General Comments. Instrumental methods used for characterization and spectroscopic studies, DFT computational details, X-ray structures, stepwise synthesis of compound [{Pt(μ-Cl)(Cl-C^C*)}$_2$] (**C**) and spectroscopic data for **1A**–**1C** and **2A**–**2C** are contained in the Supporting Information. All chemicals were used as supplied and [{Pt(μ-Cl)(NC-C^C*)}$_2$] (**A**)[29] and [{Pt(μ-Cl)(EtO_2C-C^C*)}$_2$] (**B**)[25] were prepared following the literature procedures.

Synthesis and characterization.

[Pt(NC-C^C*)(acac)] (1A). Tlacac (146.2 mg, 0.48 mmol) was added to a yellow suspension of **A** (207.2 mg, 0.25 mmol) in dichloromethane (40 mL) at r.t. After 4 h stirring, the resulting mixture was filtered through Celite, washed with dichloromethane (120 mL) and evaporated to dryness. Addition of methanol (3 x 5 mL) to the residue rendered a solid which was recrystallized by redissolving in 15 mL of dichloromethane/diethyl ether (3:1), filtering through Celite and evaporating to dryness. Addition of methanol (3 x 5 mL) to the residue rendered **1A** as a pure white solid. Yield: 178.2 mg, 78%. Elemental analysis Calcd (%) for $C_{16}H_{15}N_3O_2Pt$: C 40.34, H 3.17, N 8.82; found: C 40.20, H 3.43, N 8.78. MS MALDI (+): m/z: 476.1 $[M]^+$.

[Pt(EtO$_2$C-C^C*)(acac)] (1B). It was prepared following the method described for **1A.** Tlacac (63.4 mg, 0.21 mmol) and **B** (100.1 mg, 0.11 mmol). **1B**: white solid, yield: 80.4 mg, 71%. Elemental analysis Calcd (%) for $C_{18}H_{20}N_2O_4Pt$: C 41.30, H 3.85, N 5.35; found: C 41.04, H 3.90, N 5.32. MS MALDI (+): m/z: 523.2 $[M]^+$.

[Pt(Cl-C^C*)(acac)] (1C). It was prepared following the method described for **1A.** Tlacac (98.2 mg, 0.32 mmol) and **C** (153.9 mg, 0.17 mmol). **1C**: white solid, yield: 120.2 mg, 72%. Elemental analysis Calcd (%) for $C_{15}H_{14}N_2Cl_2O_2Pt$: C 34.63, H 2.71, N 5.39; found: C 34.29, H 2.70, N 5.36. MS MALDI (+): m/z: 520.1 $[M]^+$.

[{Pt(NC-C^C*)(acac)}$_2$Tl]PF$_6$ (2A). $TlPF_6$ (26.6 mg, 0.074 mmol) was added to a solution of **1A** (70.3 mg, 0.15 mmol) in a mixture of dichloromethane and acetone (20 mL/ 5 mL). After 2.5 h stirring in the dark, the solvent was removed under reduced pressure and the residue was treated with diethyl ether (20 mL) and filtered, to give **2A** as a yellow solid. Yield: 73.4 mg, 76%. Elemental analysis Calcd (%) for $C_{32}H_{30}F_6N_6O_4PPt_2Tl$: C 29.52, H 2.32, N 6.45; found: C 29.63, H 2.43, N 6.60. MS MALDI (+): m/z: 680.2 [Pt(NC-C^C*)(acac)Tl]$^+$.

[{Pt(EtO$_2$C-C^C*)(acac)}$_2$Tl]PF$_6$ (2B). It was prepared following the method described for **2A**. $TlPF_6$ (27.7 mg, 0.077 mmol) and **1B** (80.4 mg, 0.15 mmol). **2B**: bright yellow solid, yield: 84.1 mg, 78%. Elemental analysis Calcd (%) for $C_{36}H_{40}F_6N_4O_8PPt_2Tl$: C 30.97, H 2.89, N 4.01; found: C 30.64, H 2.71, N 4.21MS MALDI (+): m/z: 1251.6 $[M]^+$; 727.2 [Pt(EtO$_2$C-C^C*)(acac)Tl]$^+$.

[{Pt(Cl-C^C*)(acac)}$_2$Tl]PF$_6$ (2C). It was prepared following the method described for **2A**. $TlPF_6$ (29.7 mg, 0.083 mmol) and **1C** (86.0 mg, 0.17 mmol). **2C**: pale yellow solid, yield: 85.8 mg, 75%. Elemental analysis Calcd (%) for $C_{30}H_{28}Cl_4F_6N_4O_4PPt_2Tl$: C 25.92, H

2.03, N 4.03; found: C 25.66, H 1.82, N 4.21. MS MALDI (+): m/z: 1245.2 $[M]^+$, 725.0 $[Pt(Cl\text{-}C\hat{}C^*)(acac)Tl]^+$.

RESULTS AND DISCUSSION

Stepwise synthesis of compounds [Pt(R-C^C*)(acac)] (R = CN 1A, CO_2Et 1B, Cl 1C)

The *β*-diketonate compounds [Pt(R-C^C*)(acac)] (**1A**–**1C**) were synthesized by reaction of the corresponding chlorine bridged compounds $[\{Pt(\mu\text{-}Cl)(R\text{-}C\hat{}C^*)\}_2]$ (R = CN **A**, CO_2Et **B**, Cl **C**) with Tl(acac) in 1:2 molar ratio (see Experimental Section and Scheme 1, path a), which led to the precipitation of TlCl and formation of the neutral complexes **1A**–**1C**. This procedure was reported by us for the synthesis of the analogous compound derived from 3-methyl-1-(naphthalen-2-yl)-1*H*-imidazol-2-ylidene,[26] although compound **1A** was already reported and prepared by Egen *et al* following a different procedure.[30]

The synthetic procedure of **1A**–**1C** requires the availability of the dichloro bridged complexes **A**–**C.** Then, the new compound **C** was prepared following the step by step method used previously for **A** and **B**[25, 29] (see SI: description, Scheme S1 and Figures S1-S4). The IR spectra of compounds **1A**–**1C** show two υ(C=O) stretching vibrations at significantly lower energies than those found for the free ligand (*ca*.1720 cm^{-1}) which are indicative of the diketonate chelation to the metal center.[26]

Their ^1H and ^{13}C NMR spectra show the expected signals for the cyclometalated NHC group and evidence the non-equivalence of the two halves of the *β*-diketonate ligand, as correspond for a chelate coordination, (see NMR data and Figure S5 in the SI). The ^{195}Pt NMR spectra exhibit the corresponding singlets at about –3400 ppm for **1A** and **1B** and at –3167 ppm for **1C**. As shown in Figure S6, the platinum signal is less shielded in **1C**

(downfield shift of ~ 300 ppm) when compared with the others, probably due to the more electron-withdrawing character of the Cl-C^C* ligand.

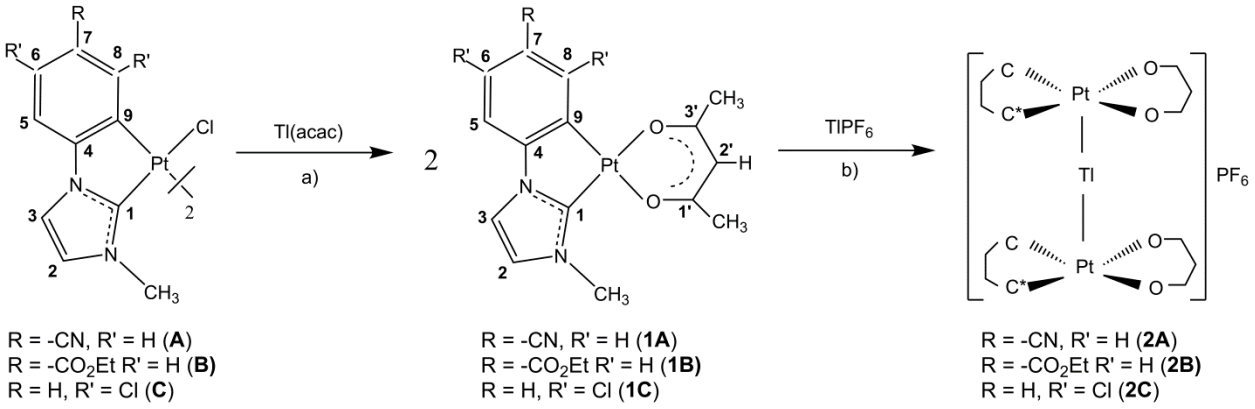

Scheme 1. Synthesis of compounds and numerical scheme for NMR purposes.

The molecular structures of **1B** and **1C** were determined by single-crystal X-ray diffraction (Figures 1 and S7). In both the two complexes, the platinum(II) center exhibits a distorted square-planar environment due to the small bite angle of the NHC cyclometalated ligand (C^C*) [ca. 80.0°]. A chelate diketonate ligand, with O-Pt-O angle close to 90°, completes the coordination sphere of Pt(II). The Pt-C* bond length [1.945(6) **1B**, 1.946(3) Å **1C**] is shorter than the Pt-C_{Ph} one [1.976(5) Å **1B**, 2.015(3) Å **1C**], as usual in compounds with cyclometalated NHCs groups.[25-26, 29, 31-35] Also, the Pt-O distances are similar to those found in related complexes.[26-27] In the solid state, complex **1B** arranges together in pairs, in a head to tail fashion through intermolecular Pt···Pt (3.370 Å) and π - π (~ 3.43 Å) interactions between the NHC ligand and the acac (see Figure 1b).[26] However, in **1C**, neither, Pt···Pt nor π···π intermolecular interactions were observed in the crystal, but C-H···Cl short contacts, as can be seen in SI (Figure S8).

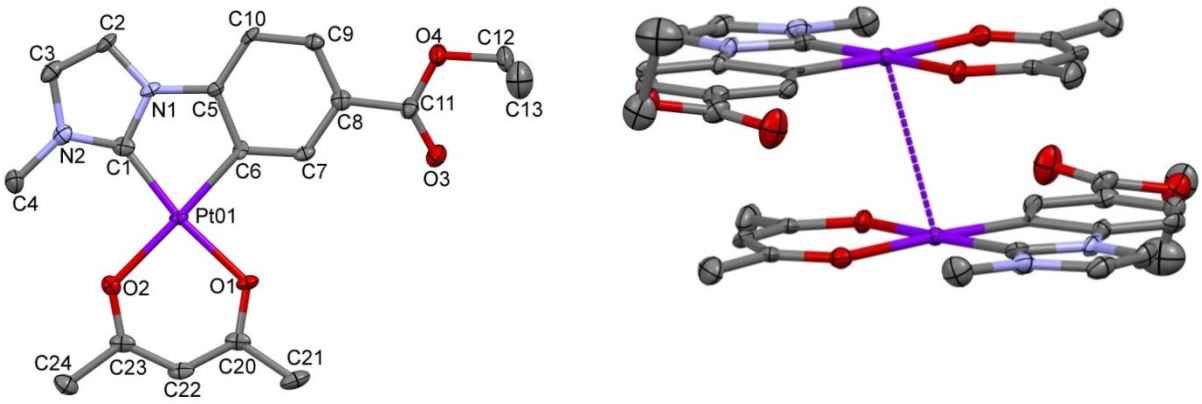

(a) (b)

Figure 1. a) Molecular structure of **1B**. Selected bond lengths (Å) and angles (deg): Pt01-C(1) 1.945(6); Pt01-C(6) 1.976(5); Pt01-O(1) 2.046(4); Pt01-O(2) 2.075(4); C(1)-Pt01-C(6) 80.4(2); O(1)-Pt01-O(2) 91.39(16); C(1)-Pt01-O(2) 97.1(2); C(6)-Pt01-O(1) 90.98(19). b) Dimer-like stacking view of **1B** (d Pt-Pt = 3.370 Å). Thermal ellipsoids are drawn at the 50% probability level. Hydrogen atoms have been omitted for clarity.

Synthesis and characterization of the clusters [{Pt(R-C^C*)(acac)}$_2$Tl](PF$_6$) (R = CN 2A, CO$_2$Et 2B, Cl 2C)

Treatment of the *β*-diketonate compounds [Pt(R-C^C*)(acac)] (R = CN **1A**, CO_2Et **1B**, Cl **1C**) with $TlPF_6$ (2:1 molar ratio) in CH_2Cl_2/acetone led to the clusters [{Pt(R-C^C*)(acac)}$_2$Tl]PF_6 (R = CN **2A**, CO_2Et **2B**, Cl **2C**), which were obtained as analytical pure solids in good yield and characterized by ^{1}H NMR, IR, mass spectrometry (see Experimental Section, Scheme 1 (path b) and SI) and X-ray crystallography. Their MALDI(+) spectra show the molecular peaks associated with [{Pt(R-C^C*)(acac)}$_2$Tl]$^+$ and [Pt(R-C^C*)(acac)Tl]$^+$, which might suggest the integrity of the trimetallic species. However, in solution at room and low (- 80ºC) temperatures, the ^{1}H and ^{195}Pt{^{1}H} NMR

spectra of **2A**–**2C** fit to those of their corresponding starting materials (see $^{195}Pt\{^{1}H\}$ NMR spectra of **2A** in Figure S9), indicating the breakdown of the Pt-Tl bonds. The photophysical data (see below) of all of these compounds were investigated and are in agreement with the rupture of the Pt-Tl bonds in solution.

The X-ray crystal structures of **2A**, **2B** and **2C** were performed on single crystals obtained from solutions of them in acetone (**2A**, **2B**) or CH_2Cl_2 (**2C**) (Table 1 and Figures 2–4). As can be seen, compounds **2A–2C** show a "Pt_2Tl" sandwich structure, where two slightly distorted square planar "Pt(R-C^C*)(acac)" subunits are bonded to a Tl(I) center through Pt-Tl bonds. In each complex, the two Pt→Tl bonds exhibit intermetallic distances slightly different from one to another (3.0499(3) Å, 3.2164(3) Å **2A**; 2.9431(4) Å, 3.0758(3) Å **2B**; 2.9962(2) Å, 3.0230(2) Å **2C**) but all of them are in the range of those observed in complexes containing Pt(II)-Tl(I) donor-acceptor bonds with no bridging ligands between the metal centers.[10]

In case of **2A** and **2B**, the Pt-Tl vectors are almost perpendicular to the Pt coordination planes (angles with the normal: 18.9(1)º Pt1A, 5.7(1)º Pt1B, **2A**; 11.4(2)º Pt1A, 10.8(1)º Pt1B, **2B**), which reveal an almost square pyramidal environment around the platinum center with the thallium atom being located on the apical position shared by both the two pyramids with a Pt-Tl-Pt angle of 169.813(9)º **2A** and 144.512(18)º **2B**.

In these compounds the platinum coordination planes are almost parallel (interplanar angle: 14.8(1)º **2A**, 34.8(2)º **2B**) but lie somewhat staggered [torsion angle O1A-Pt1A-Pt1B-O1B: 40.6º **2A**, 90.7º **2B**]. In case of **2A** an additional acetone molecule interacts with the Tl(I) center through a weak Tl-O bond (2.7692(42) Å). The Tl-O separation is comparable to

those in other complexes[10, 15, 19, 36] but significantly longer than the sum of the covalent radii (2.21 Å).[23]

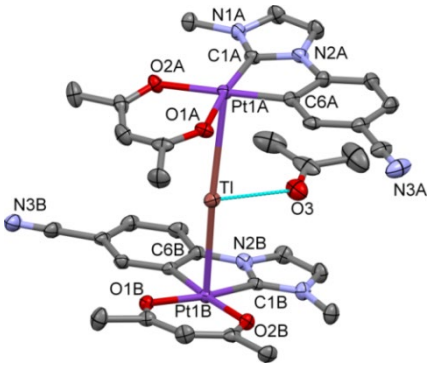

(a)

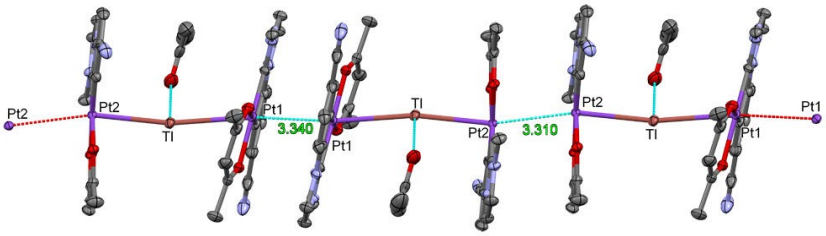

(b)

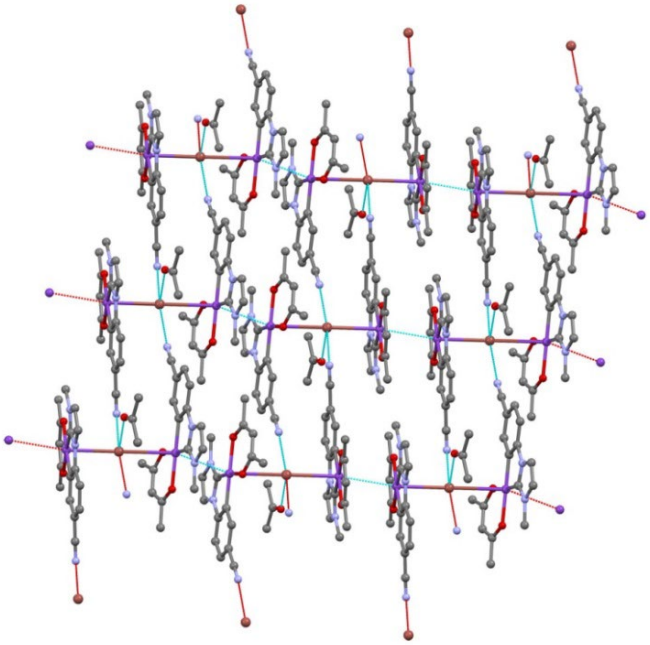

(c)

Figure 2. a) Molecular structure of **2A**. Thermal ellipsoids are drawn at the 50% probability level. Hydrogen atoms and PF_6 have been omitted for clarity. b, c) Supramolecular structure views.

The trinuclear "Pt_2Tl" units rearrange in the crystal generating 2D networks through additional stabilizing contacts. On one hand, the "Pt_2Tl" units stack through intermolecular Pt···Pt (3.340 Å, 3.310Å **2A**; 3.401 Å, 3.240Å **2B**) interactions[37-43] and weak π - π contacts between the NHC and the acac ligands[26] (the shortest atomic separation between two neighboring units is 3.467 Å **2A**; 3.429 Å **2B**, see Figures 2b and 3b), giving rise to almost linear PtB-Tl-PtA··PtA-Tl-PtB···PtB wires in **2A** [angles: PtB-Tl-PtA: 169.813º, Tl-PtA··PtA: 158.77º, Tl-PtB···PtB: 165.32º] and zig-zag chains in **2B** [angles: PtB-Tl-PtA: 145.512º, Tl-PtA··PtA: 177.80º, Tl-PtB···PtB: 160.07º]. These chains appear linked together through two additional Tl-E (E') (E, E' = N **2A**, O **2B**) bonds with the R substituents of the R-C^C* groups (R= CN **2A**, CO_2Et **2B**) belonging to the two adjacent chains (see Figures 2c and 3c). The Tl-N (NC-C^C*) and Tl-O (CO_2Et-C^C*) distances are longer than expected for covalent bonds but shorter than the sum of the covalent radii of Tl^I (1.55 Å) and the van der Waals radii of N (1.55 Å) and O (1.52 Å).[44] The Tl···N separations are comparable to those found in derivatives containing Tl···N interactions, such as [PtTl(C^N)$(CN)_2$](C^N = 7,8-benzoquinolinate (bzq), 2-phenylpyridinate (ppy)) or [{PtTl(bzq)$(CC\text{-}C_5H_4N\text{-}2)_2\}_2$][13] and [*trans,trans*,*trans*-$Tl_2\{Pt(C_6F_5)_2(CN)_2\}(CH_3COCH_3)_2]_n$.[19] Then, the five-coordinated Tl(I) center in **2A** is located in the middle of the base of a square-pyramid with bond angles around the Tl(I) center close to 90º [angles: Pt1A-Tl-N3B: 92.0º, Pt1B-Tl-N3B: 95.0º, Pt1A-Tl-N3A: 81.2º, Pt1B-Tl-N3A: 93.3º, O3-Tl-N3B: 89.5º, O3-Tl-N3A: 101.6º, Pt1A-Tl-O3: 86.2º, Pt1B-Tl-O3: 86.5º]. Single crystals

of **2B** were also obtained from an acetone solution, however in this case the Tl(I) center does not coordinate any acetone molecule and exhibits a distorted tetrahedral coordination environment [angles: Pt1A-Tl-O3A: 108.5.0º, Pt1A-Tl-O3B: 110.8º, Pt1B-Tl-O3A: 93.1º, Pt1B-Tl-O3B: 87.8º, O3A-Tl-O3B: 107.6º].

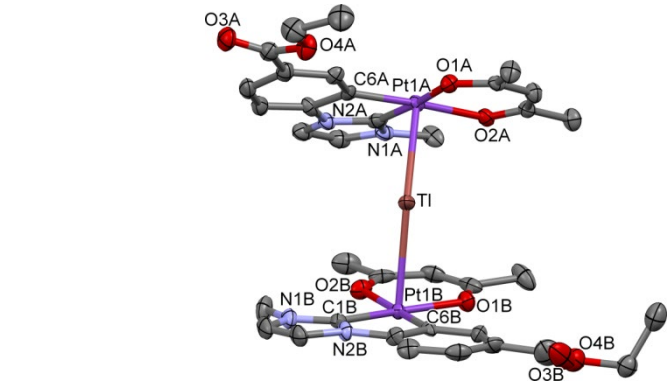

(a)

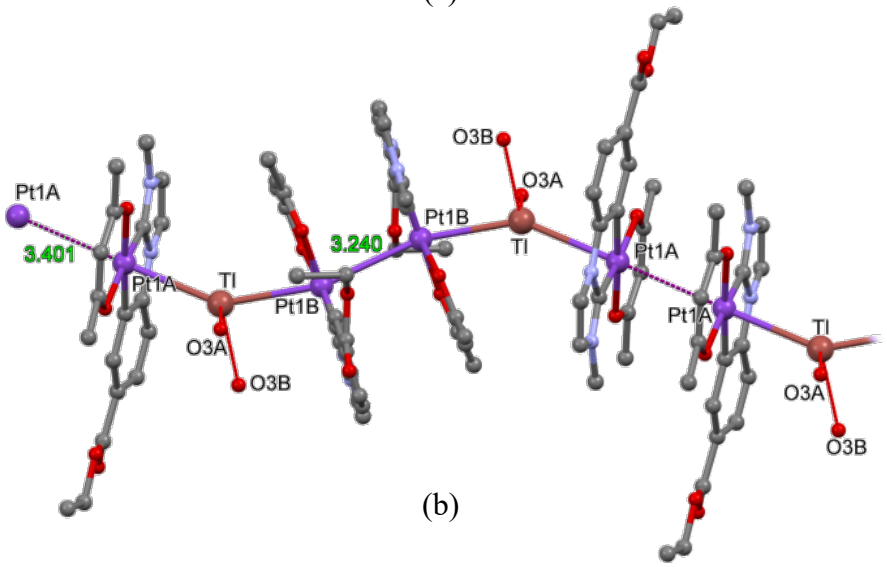

(b)

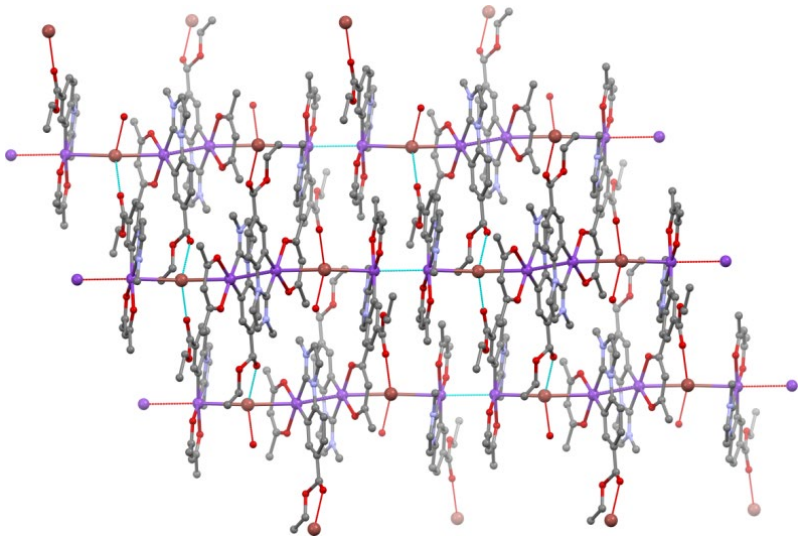

(c)

Figure 3. a) Molecular structure of **2B**. Thermal ellipsoids are drawn at the 50% probability level. Hydrogen atoms and PF_6 have been omitted for clarity. b and c) Supramolecular structure views.

Compound **2C**, unlike **2A** and **2B**, is a discrete molecule and not a 2D lattice, because of the absence of intermolecular or packing interactions (see Figure S10). In compound **2C**, the Tl(I) in addition to the two Pt-Tl bonds (d Pt-Tl: 3.0230(2) Å, 2.9962(2) Å; Pt-Tl-Pt: 119.475(8)º), establishes two intramolecular Tl···Cl contacts (d Tl···Cl = 3.3237(1) and 3.5717(4) Å), one with each of the "Pt(Cl-C^C*)(acac)" fragments, a Tl···F contact (d Tl···F = 3.063 Å) with the anion and a Tl···Cl contact (d Tl··Cl = 3.497 Å) with a CH_2Cl_2 molecule, to complete a distorted octahedral coordination environment (Figure 4b). All the Tl-E (E = Cl, F) distances are rather long, but lower than the sum of the van der Waals radii of Tl(I) (1.96 Å), and F (1.47 Å) or Cl (1.75Å).[44] In this molecule, the Pt-Tl vectors are further away from the perpendicular to the Pt coordination planes (angles: 25.2(1)º Pt1A, 19.6(1)º Pt1B) than in compounds **2A** and **2B** and the angle Pt-Tl-Pt (119.475(8)º) is far

away from the ones observed in **2A** and **2B**, probably forced by the existence of the two intramolecular Tl···Cl contacts.

Table 1. Selected bond lengths (Å) and angles (º) for complexes **2A–2C**

	2A	**2B**	**2C**
Pt(1A)-C(1A)	1.947(5)	1.953(9)	1.958(5)
Pt(1A)-C(6A)	1.979(5)	1.994(8)	2.023(4)
Pt(1A)-O(1A)	2.050(3)	2.059(5)	2.042(3)
Pt(1A)-O(2A)	2.069(4)	2.073(6)	2.051(4)
Pt(1B)-C(1B)	1.939(5)	1.956(8)	1.951(4)
Pt(1B)-C(6B)	1.988(5)	1.993(8)	2.010(4)
Pt(1B)-O(1B)	2.058(3)	2.069(6)	2.052(3)
Pt(1B)-O(2B)	2.075(3)	2.063(6)	2.054(3)
Pt(1A)-Tl	3.2164(3)	3.0758(4)	3.0230(2)
Pt(1B)-Tl	3.0499(3)	2.9431(4)	2.9962(2)
Tl-E	2.8970(51)	2.7715(67)	3.3237(1)
	(E= N3A)	(E= O3A)	(E= Cl1A)
Tl-E’	2.9942(48)	2.8419(77)	3.5717(4)
	(E’= N3B)	(E’= O3B)	(E’= Cl1B)
Tl-E’’	2.7692(42)		3.0633(4)
	(E’’= O3)		(E’’= F4)
Tl-E’’’			3.497(4)
			(E’’’= Cl4)
Pt(1A)···Pt(1A')	3.340(1)	3.401(1)	
Pt(1B)···Pt(1B')	3.310(1)	3.240(1)	
Pt(1A)-Tl-Pt(1B)	169.813(9)	144.512(18)	119.475(8)
C(1A)-Pt(1A)-C(6A)	80.0(2)	80.2(3)	80.04(19)
O(1A)-Pt(2A)-O(2A)	90.20(14)	90.5(2)	89.34(15)
C(1B)-Pt(1B)-C(6B)	79.8(2)	80.6(3)	80.07(18)
O(1B)-Pt(2B)-O(2B)	91.04(13)	91.2(2)	89.09(13)

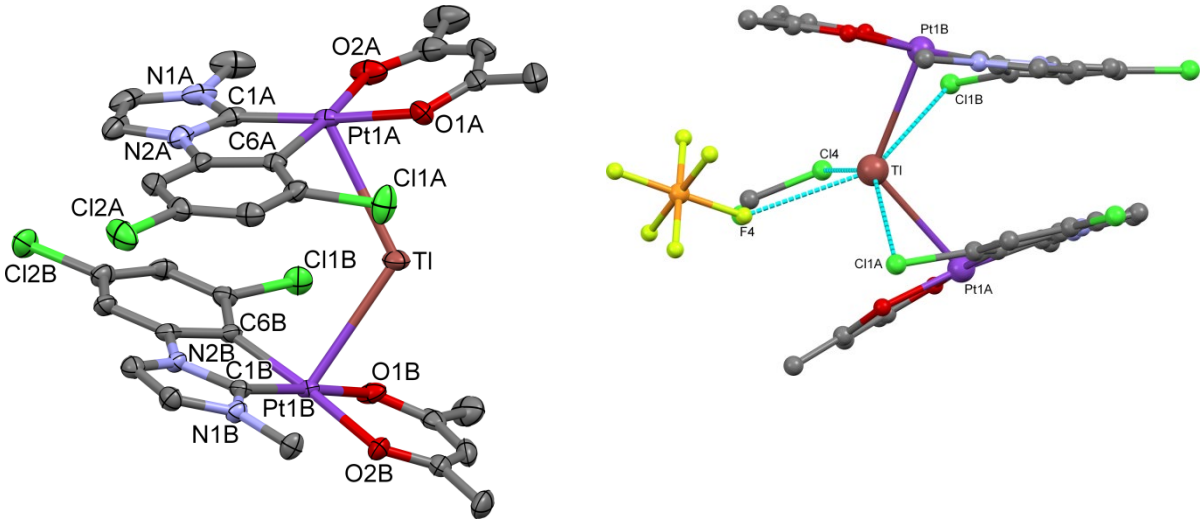

(a) (b)

Figure 4. (a) Molecular structure of **2C**. Thermal ellipsoids are drawn at the 50% probability level. Hydrogen atoms have been omitted for clarity. (b) Structure view of the Tl···E interactions.

It should be noted that in **1B,** the molecules arrange themselves in dimers through Pt···Pt interactions, not giving rise to 1D wires, as observed in **2B** and **2A**. Presumably, the Pt-Tl donor acceptor bond decreases the electron density on the platinum, playing a similar role to that of π-acceptor ligands, thereby reducing electronic repulsions between the Pt centers and favoring the 1D chain formation through Pt···Pt interactions.[45-47]

Photophysical properties of compounds [Pt(R-C^C*)(acac)] (R = CN 1A, CO_2Et 1B, Cl 1C) and the corresponding clusters [{Pt(R-C^C*)(acac)}$_2$Tl]PF_6 (2A–2C).

The photophysical properties of **1A** were previously described by Da Como *et al*[48] but we have included them in this discussion with comparative purposes.

Absorption spectra.

UV-Vis spectroscopic data of compounds **1A**–**1C** and **2A**–**2C** have been listed in Table S1. The spectra of **1A**–**1C** in solution of CH_2Cl_2 (see Figure S11) display low intensity absorptions ($\varepsilon > 10^3$ M^{-1} cm^{-1}) at low energies ($\lambda > 290$ nm). In case of **1C**, they appear clearly shifted to higher energies with respect to those of **1A** and **1B**, indicating the participation and the effect of the R-C^C* (R = CN, CO_2Et, Cl) group in these absorptions. In case of **1A**, these absorptions are very similar to those of **1B** in energy and profile, in agreement with the similar electronic features observed previously for the R-C^C* (R = CN, CO_2Et) groups.[24]

The solid-sate diffuse reflectance UV-Vis spectra (Figure S12) show additional broad bands at low energy when compared with those observed in dichloromethane solution, which can be tentatively attributed to the existence of intermolecular Pt-Pt interactions, on the light of the X-ray structure of **1B** and those of other related complexes.[26]

DFT and TD-DFT calculations in solution of CH_2Cl_2 for **1B** and **1C** have been carried out to provide correct assignments for the UV-Vis absorptions and also to evaluate the effect of the cyclometalated R-C^C* group (see full data in SI). Considering the composition of the frontier molecular orbitals (FOs), the calculated allowed absorptions, which are in good agreement with the experimental UV-vis spectra (Figure S14), and the origin of calculated S_1, which arises mainly from a HOMO to LUMO transition (79% **1B**, 62% **1C**), the lowest energy absorption band can be attributed basically to L'LCT [π(acac) → π*(NHC)] transitions for **1C,** and mixed L'LCT [π(acac) → π*(NHC)] / MLCT [5d(Pt) → π*(NHC)] transitions for **1B**. Although S_2 arises mainly from an H-1 to LUMO transition, it is very similar in nature to S_1. Taking into account the similarities in the electronic features of the

R-C^C* (R = CN, CO_2Et) groups observed in the absorption spectra of **1A** and **1B** as well as in those of other compounds reported previously,[24] the nature of the lowest energy absorptions of **1A** are expected to be quite similar in nature to those of **1B**.

The absorption spectra of complexes **2A**–**2C** in 2-MeTHF solutions (10^{-4} M) are all identical to those of their respective precursors, **1A**–**1C** (see Figure S15), which match with the rupture of the Pt-Tl bonds in solution, as deduced from their NMR spectra. Similar behavior was previously observed in related extended structures with M–Tl bonds [M(C^N)$(CN)_2$Tl] (M = Pt,[13] Pd,[26] C^N = 7,8-benzoquinolinate, 2-phenylpyridinate). The absorption spectra of powdery solid samples of **2A**–**2C** basically fit with those of the starting materials (Figure S16). In the low-energy region just **2B** displays and additional absorption with respect to its precursor, with λ_{max} at 400 nm (see Figure 5). Keeping in mind the shorter Pt-Tl and Pt···Pt distances in the network of **2B** compared to those of **2A**, this absorption could be attributed to metal-metal-to ligand charge transfer (^{1}MMLCT) [dσ*(Pt-Pt)→ π*(NHC)] transitions likely to have been affected by the Pt-Tl bonds.

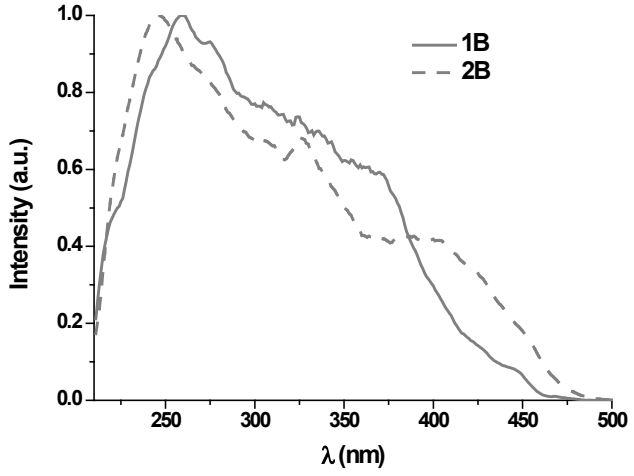

Figure 5. Normalized Diffuse Reflectance spectra of powdery solid samples of **1B** and **2B** at r.t.

Emission Spectra. Emission data are summarized in Table 2. In diluted glassy solutions of 2-MeTHF (10^{-5} M, 77 K), compounds **1A–1C** show blue well resolved vibronic emissions (see Figure S17) that do not change at higher concentration (10^{-3} M, Figure S18). Their vibrational spacings [1367–1406 cm^{-1}] correspond to the C=C/C=N stretches of the cyclometallated NHC ligand (C^C*), suggesting their involvement in the excited state. The emissions of **1A** and **1B** (λ_{max}~ 440 nm) are red shifted with respect to that of **1C** (λ_{max} = 417 nm), probably due to the participation of the R-substituent in the stabilization of the LUMO, as revealed by the DFT studies. Emissions and lifetime decays of **1A** and **1B** are identical to those observed in [(R-C^C*)Pt(py)(PPh_3)]PF_6[24] and very similar [(R-C^C*)Pt(CNR')]PF_6[25] which contain the same "(R-C^C*)Pt" fragments. Thus, taking into account all this and the TD-DFT calculations, the phosphorescent emissions of **1A–1C** can be mainly ascribed to transitions of monomeric species derived from ^{3}ILCT [(NHC)] transitions mixed with some, if any, ^{3}L'LCT [π(acac) → π*(NHC)] / ^{3}MLCT [5d(Pt) → π*(NHC)] in the case of **1A** and **1B** and with ^{3}L'LCT [π(acac) → π*(NHC)] for **1C**.

Emission spectra for the 5 wt% films of complexes **1A–1C** in poly(methyl methacrylate) (PMMA) are wavelength dependent, as can be shown in Figure 6. Upon excitation at λ = 330 nm, all the three compounds show a phosphorescent emission in the blue to green region of the visible spectrum, like in glassy 2-MeTHF, with quantum yields up to 0.93 (**1B**), very similar to that of **1A** (0.98), while just 0.04 for **1C** (Table 2). However, upon excitation at λ > 390 nm, there is a dramatic change in the emission profiles whereby a low-energy (LE) structureless band with maxima at *ca*. 540 nm becomes predominant while the HE is still observed but as a low intensity shoulder.

Table 2. Emission data for complexes **1A–2C.**

C.	Medium (T/K) [wt%]	λ_{ex}/nm	λ_{em}/nm	τ/μs [λ_{max}][a]	ϕ
1A	PMMA film [5 wt%][b]	330	441, 470_{max}, 503, 536_{sh}		0.98
		390	443, 474, 535_{max}		0.72
	PMMA film [40 wt%][b]	330	443, 474, 535_{max}		0.46
	Solid (298 K)	400	462_{sh}, 479_{max}, 513, 555	0.28 (77%), 0.65 (23%)	0.04
	Solid (77 K)	400	451, 477, 512_{max}	0.78 (70%), 3.1 (30%) [451],	
				0.35 (55%), 1.2 (45%) [512]	
	2-Me-THF (77 K)[c]	332	439_{max}, 468, 500, 523_{sh}	17.1	
1B	PMMA film [5 wt%][b]	330	446, 474_{max}, 502, 536_{sh}		0.93
		390	452, 484_{sh}, 532_{max}		0.59
	PMMA film [40 wt%][b]	330	452, 484_{sh}, 532_{max}		0.82
	Solid (298 K)	400	485_{max}, 519, 550	2.1 (60%), 1.0 (40%) [485]	0.48
				1.5 (83%), 2.8 (17%) [519]	
	Solid (77 K)	400	461, 495, 554_{max}	2.6 [461], 3.8 [554]	
	2-Me-THF (77 K)[c]	332	442_{max}, 472, 502, 536_{sh}	16.9	
1C	PMMA film [5 wt%][b]	330	425, 450_{max}, 475		0.04
		400	540		0.09
	Solid (298 K)	380	433, 452_{max}, 476, 516	3	0.07
	Solid (77 K)	380	432, 456_{max}, 482, 515_{sh}	11.6	
	2-Me-THF (77 K)[c]	320	417_{max}, 443, 472, 500_{sh}	15.6	
2A	Solid (298 K)	380	450, 478_{max}, 506	0.64 [450]	0.17
				0.43(80%), 1.44 (20%) [478]	
				0.44 (77%), 1.8 (23%) [506]	
	Solid (77 K)	380	500	1.7	
	2-Me-THF (77 K)[c]	330	439_{max}, 469, 500, 524_{sh}	16.5	
2B	Solid (298 K)	474	580	0.31 (67%), 1.15 (33%)	0.02
	Solid (77 K)	474	561	0.95	
	2-Me-THF (77 K) [c]	332	443_{max}, 473, 505, 534_{sh}	16.7	
2C	Solid (298 K)	351	425, 450_{max}, 480, 514	1.3 (54%), 2.4 (46%) [450]	0.10
				1.8 [480], 1.9 [514]	
	Solid (77 K)	343	421_{sh}, 448_{sh}, 494_{max}	3.3 (44%), 8.6 (56%) [494]	
	2-Me-THF (77 K) [c]	320	417_{max}, 444, 472, 501_{sh}	13.2	

a = Lifetime measured at the λ_{max}. b: 298 K. c = 10^{-5} M; at 10^{-3} M, the same emission and τ were obtained.

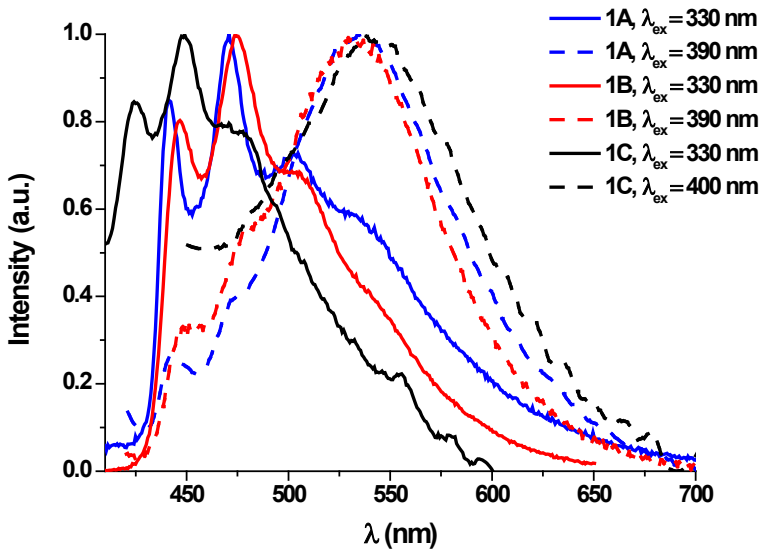

Figure 6. Normalized emission spectra of **1A**–**1C** in 5 wt % PMMA film

Intrigued by this behavior, we carried out further experiments only focused on **1A** and **1B** since **1C** is barely emissive. Therefore, their emission spectra were registered in PMMA coated films at different weight concentration ranging from 0.5 wt% to 40 wt%. As can be seen in Figure 7 (**1B**) and Figure S19 (**1A**), pure highly structured emissions were found at concentration 0.5 wt%. When increasing the weight percentage of the complex in the PMMA film, the intensity of the LE increases and that of the HE band decreases, resulting in a green emission as much for 20 wt% as for 40 wt% films. At 40 wt%, the green emission shows no dependence with the λex (see Figure S20).

At 40 wt% concentration the QY values of the green emission kept fairly high for **1B** (0.82) while the emission of **1A** (QY = 0.46) became slightly self-quenched. In all likelihood, the LE bands can be attributed to metal-metal-to ligand charge transfer (^{3}MMLCT) [dσ*(Pt-Pt) → π*(NHC)] transitions, generated by the existence of aggregates in the ground state through Pt–Pt interactions, as observed in the X-ray structure of **1B**. The excimeric nature

of this LE emission is discarded since the excitation spectrum of **1B** in PMMA film at 40 wt% is very similar to that obtained for the solid state one (see Figure S21). Therefore , the dual emission observed in PMMA films of **1A-1C** is likely due to a relatively slow internal conversion between the two emissive states ^{3}ILCT(NHC)/^{3}MMLCT at 298 K.[11]

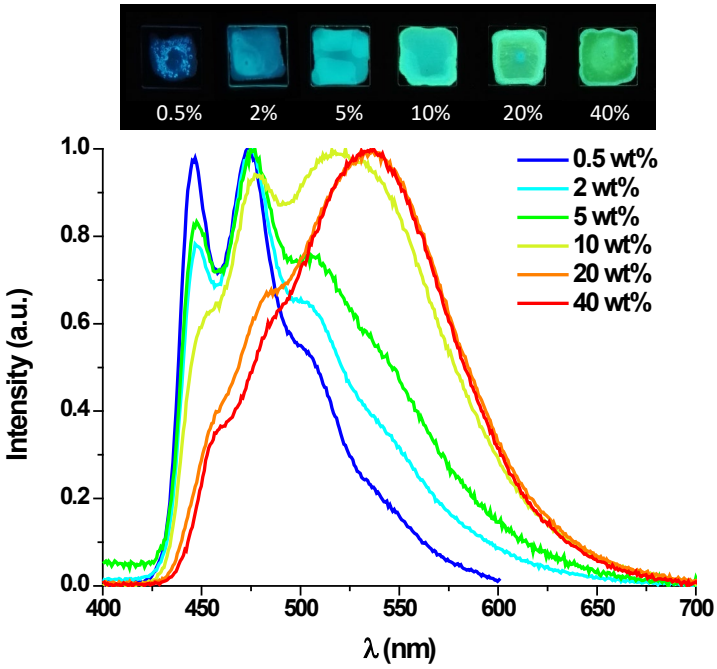

Figure 7. Normalized emission spectra of **1B** at λex = 360 nm. Pictures under UV light (λ_{ex} = 365 nm).

In solid state, powdery samples of **1A–1C** display bright blue and greenish blue emissions (λ_{max} ~ 480 nm for **1A** and **1B**; λ_{max}= 452 nm for **1C**) with the emission of compound **1C** located further into the blue region of the spectrum than the others (Figure S22). Upon cooling to 77 K, the emission of **1C** appears a bit more structured and with a longer

lifetime, being quite similar to the one obtained in 2-MeTHF solution (Figure 8).

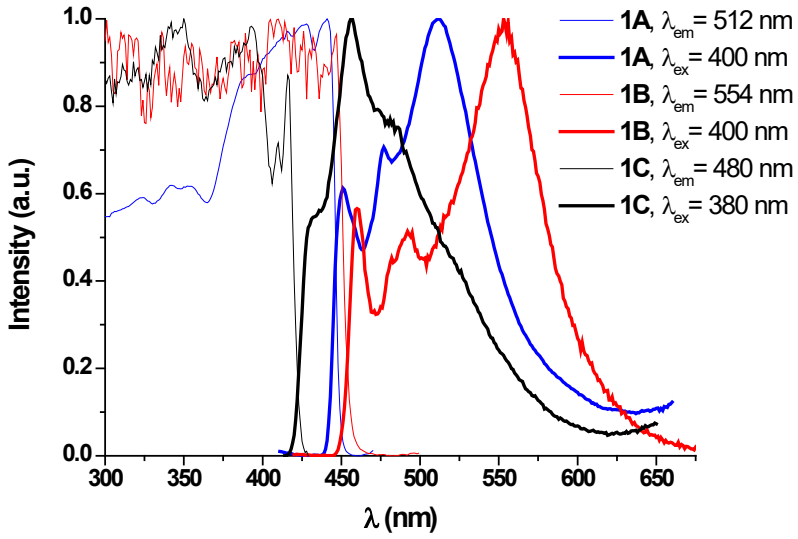

Figure 8. Normalized excitation (—) and emission (**▬**) spectra of **1A–1C** in solid state at 77 K.

However, both **1A** and **1B** (see Figure 8), regardless the excitation wavelength (350 to 450 nm), display broad bands with λ_{max} = 512 and 554 nm, respectively, accompanied by high energy (HE) structured emissions at 451 (**1A**) and 461 (**1B**) nm. These HE bands resemble to those obtained in PMMA films with a low doping concentration (< 5 wt%) and in solution of 2-MeTHF. Likewise, the LE bands of **1A** (512 nm) and **1B** (554 nm) are closely related to those obtained in PMMA films (> 10 wt% and λex > 360 nm). Therefore, these dual emissions (HE and LE bands) may come from the excited states discussed above (^{3}ILCT [(NHC)] and ^{3}MMLCT, respectively).

The emissive behavior of the Pt_2Tl clusters, **2A**–**2C**, was investigated to compare it with that of **1A**–**1C**. As expected, in glassy solutions of 2-MeTHF compounds **2A**–**2C** give the same emission bands and lifetime decays than **1A**–**1C** either at diluted (10^{-5} M) or

concentrated solutions (10^{-3} M), which once again, evidences the rupture of the M–Tl bonds in solution even at 77 K (Figure S23). Emission spectra of **2A**–**2C** in 5 wt% PMMA films closely resemble those of their corresponding precursors, **1A**–**1C** (see Figure S24), which pointed us to consider that in PMMA films, the Pt-Tl bonds, if present, are negligible.

In solid state at room temperature, the Pt_2Tl complexes display vibronic bands like their corresponding starting materials except **2B**, which shows a structureless broad band considerably shifted to lower energies (Figures 9 and 10), in line with the features observed in the absorption spectra of powdery samples of them (Figures 5 and S16). At 77 K the emission of **2B** becomes a narrow unstructured band at 561 nm (Figure 9).

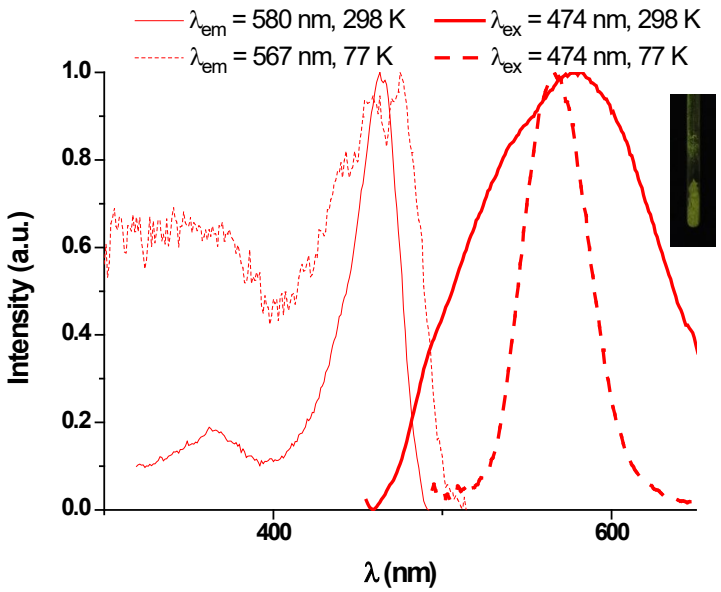

Figure 9. Normalized excitation (—) and emission (**▬**) spectra of **2B** in solid state. Picture under UV light (λ_{ex} = 365 nm) at 298 K.

Considering that the excitation spectra match the absorption one, the short lifetime decay and the X-ray structure, the emission of **2B** could be mainly attributed to ^{3}MMLCT [dσ*(Pt-Pt) → π*(NHC)] transitions somewhat disturbed by the Pt-Tl bonds.

Upon cooling to 77 K the emission profile of **2A** retains a minor contribution of the HE band but displays a predominant unstructured LE emission band at *ca*. 500 nm (Figure 10). This LE band appears just slightly blue-shifted with respect to the LE band of **1A** but it shows similar lifetime and excitation spectrum so the same ^{3}MMLCT nature can be presumed for it. It should be stressed that even though the crystal structures obtained for **2A** and **2B** show similar 2D networks, in **2A**, the presence of an extended metallic [Pt-Pt-Tl-Pt-Pt-] chain is not reflected in its absorption or emissive properties at room temperature (see Figure S25). However, at 77 K the emission of **2A** also depends on the intermolecular Pt···Pt interactions.

For **2C**, consisting of Pt_2Tl discrete molecules, the emission profile and its bi-exponential decay differ from those of the starting complex as much at 298 K as at 77 K, indicating that it is affected by the Pt-Tl bonds. At 77 K the mayor LE band appears slightly red-shifted in relation to those of other trinuclear derivatives $(NBu_4)_3[\{Pt(C_6F_5)_4\}_2Tl]$ (450 nm, 298 K; 445 nm, 77 K),[16] $[Tl_2Pt(CN)_4]$ (448 nm),[12] which were attributed to a metal-centered phosphorescence process [Pt(5dz^2) → Tl(6pz)] (^{3}MM'CT) within the trinuclear entity. The observed shift in **2C** might be attributed to the contribution of the planar and low-lying C^C* and acac ligands to the frontier orbitals, which likely reduces the gap of the transition, more than to the existence of stronger Pt−Tl bonds, as deduced by comparing intermetallic distances (2.9962(2), 3.0230(2) Å, **2C** − vs 2.9777(4), 3.0434(4) Å $[\{Pt(C_6F_5)_4\}_2Tl]_3$,]). Therefore, the emission can be tentatively ascribed to charge transfer

from the platinum fragments to the thallium [^{3}(L+L')MM'CT],[10] with some contribution of ^{3}MM'LCT/^{3}IL [d/sσ*(Pt–Tl) →π*(C^C*)] excited states. For powdery samples of **2C** at 77 K the existence of close excited states generated by small differences in the molecular arrangement can be not excluded, which could explain the huge width of the emission band.

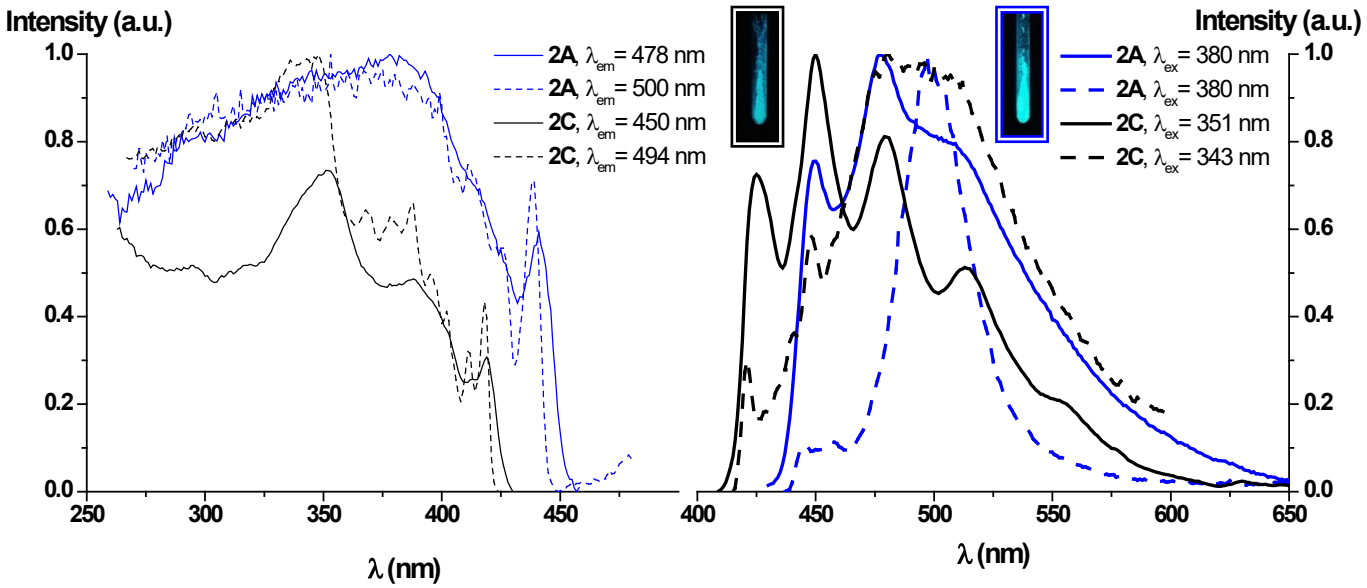

Figure 10. Normalized excitation (right) and emission (left) spectra of **2A** and **2C** in solid state at 298 K (—) and 77 K (---). Pictures under UV light (λ_{ex} = 365 nm) at 298 K.

CONCLUSIONS

The new cyclometalated NHC compound [{Pt(μ-Cl)(R-C^C*)}$_2$] (R = Cl, **C**) was successfully prepared following our stepwise protocol. From **C** and the related ones **A** (R = CN) and **B** (R = CO_2Et) the mononuclear complexes [Pt(R-C^C*)(acac)] (R = CN **1A**, CO_2Et **1B**, Cl **1C**) were obtained. They reacted with $TlPF_6$ in a 2:1 molar ratio to give the corresponding heterotrinuclear cluster [{Pt(R-C^C*)(acac)}$_2$Tl]$^+$ (**2A**, **2B**, **2C**) which are held together by donor–acceptor Pt–Tl bonds, confirming the ability of this kind of Pt(II)

complexes to act as Lewis bases for this kind of interactions. These metal-metal bonds present in the solid state, break down in solution even at low temperatures (- 80ºC).

The crystallographic, spectroscopic and photophysical study of **1A**–**1C** and their corresponding Pt_2Tl clusters discovered that electron withdrawing substituents, such as CN and CO_2Et, in the 4-position of the cyclometalated ring confer very high PLQY to the mononuclear complexes and enable the Pt_2Tl clusters to self-assemble in 2D extended lattice through intermolecular Pt–Pt, π–π, Tl–N or Tl–O interactions. By contrast, the presence of two Cl substituents in positions 3 and 5 of the cyclometalated ring severely reduces the emission efficiency of the mononuclear **1C** compared to those of **1A** and **1B** and also leads to discrete Pt_2Tl cluster (**2C**) because allows the Tl center to satisfy its electronic demand through intramolecular Tl-Cl contacts.

Complexes **1A** and **1B** show in 5wt% films in PMMA dual emissions, blue (HE) and green-yellow (LE) bands, attributed to ^{3}ILCT and ^{3}MMLCT excited states, respectively. By controlling the excitation wavelength and the concentration of the complex in the film the blue or green emissions could be finely tuned with very high PLQY (0.98–0.72). The inclusion of Tl into these systems does not improve the quantum efficiency, instead the emission of **2B** resulted to be quenched because of the existence of weakly emissive ^{3}MMLCT [dσ*(Pt-Pt) → π*(NHC)] excited states, due to the strong Pt···Pt interactions in the extended metallic [Pt-Pt-Tl-Pt-Pt-] chain.

ASSOCIATED CONTENT

The Supporting Information is available free of charge on the ACS Publications website.

General procedures and instrumentation, crystallographic and computational details; spectroscopic data, NMR spectra; X-ray crystallographic data and structures; UV-Vis data

and figures; DFT and TD-DFT calculations and emission spectra (PDF); Crystallographic data for compounds **1B**, **1C** and **2A–2C** (CIF)

AUTHOR INFORMATION

Corresponding Author

*E-mail: sicilia@unizar.es

ACKNOWLEDGMENTS

This work was supported by the Spanish Ministerio de Economía y Competitividad (MINECO)/FEDER (Project CTQ2015-67461-P led by Dr. Babil Menjón) and the Departamento de Industria e Innovación del Gobierno de Aragón and Fondo Social Europeo (Grupo Consolidado E21: Química Inorgánica y de los Compuestos Organometálicos led by Dr. José M. Casas). The authors thank the Centro de Supercomputación de Galicia (CESGA) for generous allocation of computational resources.A. C. acknowledges the support of a FPI grant from the Spanish government.

REFERENCES

1. Collman, J. P.; Hegedus, L. S.; Norton, J. R.; Finke, R. G., *Principles and Applications of Organotransition Metal Chemistry;* . University Science Books: Mill Valley, California, **1987.**

2. Crabtree, R. H., *Organometallic Chemistry of the Transition Metals, 3rd ed.* John Wiley & Sons: New York, **2001**.

3. Atwood, J. D., *Inorganic and Organometallic Reaction Mechanisms, 2nd ed.* Wiley-VCH: Weinheim, **1997**.

4. Sculfort, S.; Braunstein, P., *Chem. Soc. Rev.* **2011,** *40*, 2741-2760.

5. Moret, M.-E. *Top Organomet. Chem* **2011,** *35*, 157-184.

6. Braunstein, P.; Oro, L. A.; Raithby, P. R.,Eds. *Metal Clusters in Chemistry; Wiley-VCH Verlag GmbH*: Weinheim, Germany, **1999***; Vol 3.*

7. Bauer, J.; Braunschweig, H.; Dewhurst, R. D., *Chem. Rev.* **2012**, *112*, 4329-4346.

8. Diez, A.; Lalinde, E.; Moreno, M. T., *Coord. Chem. Rev.* **2011**, *255*, 2426-2447.

9. Baya, M.; Belío, U.; Fernández, I.; Fuertes, S.; Martín, A., *Angew. Chem. Int. Ed.* **2016**, *55*, 6978 -6982 and references therein.

10. Forniés, J.; Giménez, N.; Ibáñez, S.; Lalinde, E.; Martín, A.; Moreno, M. T., *Inorg. Chem.* **2015,** *54*, 4351-4363 and references therein.

11. Berenguer, J. R.; Lalinde, E.; Martín, A.; Moreno, M. T.; Sánchez, S.; Shahsavari, H. R., *Inorg. Chem.* **2016,** *55*, 7866- 7878.

12. Nagle, J. K.; Balch, A. L.; Olmstead, M. M., *J. Am. Chem. Soc.* **1988,** *110*, 319-321.

13. Forniés, J.; Fuertes, S.; Martín, A.; Sicilia, V.; Gil, B.; Lalinde, E., *Dalton Trans.* **2009**, 2224-2234.

14. Usón, R.; Forniés, J.; Tomás, M.; Garde, R.; Merino, R. I., *Inorg. Chem.* **1997,** *36*, 1383-1387.

15. Jamali, S.; Ghazfar, R.; Lalinde, E.; Jamshidi, Z.; Samouei, H.; Shahsavari, H. R.; Moreno, M. T.; Escudero-Adán, E.; Benet-Buchholzd, J.; Dalibor Milice, D., *Dalton Trans.* **2014,** *43*, 1105-1116.

16. Falvello, L. R.; Forniés, J.; Garde, R.; García, A.; Lalinde, E.; Moreno, M. T.; Steiner, A.; Tomás, M.; Usón, I., *Inorg. Chem.* **2006,** *45*, 2543-2552.

17. Charmant, J. P. H.; Forniés, J.; Gómez, J.; Lalinde, E.; Merino, R. I.; Moreno, M. T.; Orpen, A. G., *Organometallics* **2003,** *22*, 652-656.

18. Berenguer, J. R.; Fernández, J.; Lalinde, E.; Sánchez, S., *Chem. Commun.* **2012,** *48*, 6384-6386.

19. Forniés, J.; García, A.; Lalinde, E.; Moreno, M. T., *Inorg. Chem.* **2008,** *47*, 3651-3660.

20. Belío, U.; Fuertes, S.; Martín, A., *Dalton Trans.* **2014,** *43*, 10828-10843.

21. Berenguer, J. R.; Forniés, J.; Gil, B.; Lalinde, E., *Chem. - Eur. J.* **2006,** *12*, 785-795.

22. Berenguer, J. R.; Forniés, J.; Gómez, J.; Lalinde, -. E.; Moreno, M. T., *Organometallics,* **2001,** *20*, 4847-4851.

23. Chen, W.; Liu, F.; Xu, D.; Matsumoto, K.; Kishi, S.; Kato, M., *Inorg. Chem.* **2006,** *45*, 5552-5560.

24. Fuertes, S.; Chueca, A.; Arnal, L.; Martín, A.; Botta, C.; Giovanella, U.; Sicilia, V., *Inorg. Chem.* **2017**, 56, 4829-4839.

25. Fuertes, S.; Chueca, A. J.; Perálvarez, M.; Borja, P.; Torrell, M.; Carreras, J.; Sicilia, V., *ACS App. Mat. Interfaces* **2016,** *8*, 16160-16169.

26. Fuertes, S.; Garcia, H.; Peralvarez, M.; Hertog, W.; Carreras, J.; Sicilia, V., *Chem. Eur. J.* **2015,** *21*, 1620-1631.

27. Leopold, H.; Heinemeyer, U.; Wagenblast, G.; Münster, I.; Strassner, T., *Chem. Eur. J.* **2016,** *22*, 1-12.

28. Zhang, X.; Cao, B.; Valente, E. J.; Hollis, T. K., *Organometallics* **2013,** *32*, 752-761.

29. Fuertes, S.; Chueca, A. J.; Sicilia, V., *Inorg. Chem.* **2015,** *54*, 9885-9895.

30. Schildknecht, C.; Ginev, G.; Kammoun, A.; Riedl, T.; Kowalsky, W.; Johannes, H.-H.; Lennartz, C.; Kahle, K.; Egen, M.; Geßner, T.; Bold, M.; Nord, S.; Erk, P., Novel deep-blue emitting phosphorescent emitter. *Proc. SPIE 5937, Organic Light-Emitting Materials and Devices IX, 59370E (October 08, 2005); doi:10.1117/12.614331* **2005,** *5937*.

31. Tronnier, A.; Metz, S.; Wagenblast, G.; Münster, I.; Strassner, T., *Dalton Trans.* **2014,** *43*, 3297-3305.

32. Tronnier, A.; Nischan, N.; Metz, S.; Wagenblast, G.; Münster, I.; Strassner, T., *Eur. J. Inorg. Chem.* **2014,** *2014*, 256-264.

33. Tronnier, A.; Nischan, N.; Strassner, T., *J. Organomet. Chem.* **2013,** *730*, 37-43.

34. Hudson, Z. M.; Blight, B. A.; Wang, S. N., *Org. Lett.* **2012,** *14*, 1700-1703.

35. Unger, Y.; Meyer, D.; Molt, O.; Schildknecht, C.; Münster, I.; Wagenblast, G.; Strassner, T., *Angew. Chem., Int. Ed.* **2010,** *49*, 10214-10216.

36. Catalano, V. J.; Bennett, B. L.; Muratidis, S.; Noll, B. C., *J. Am. Chem. Soc.* **2001,** *123*, 173-174.

37. Yam, V. W. W.; Wong, K. M. C.; Zhu, N., *J. Am. Chem. Soc.* **2002,** *124*, 6506-6507.

38. Kato, M.; Kosuge, C.; Morii, K.; Ahn, J. S.; Kitagawa, H.; Mitani, T.; Matsushita, M.; Kato, T.; Yano, S.; Kimura, M., *Inorg. Chem.* **1999,** *38*, 1638-1641.

39. Buss, C. E.; Mann, K. R., *J. Am. Chem. Soc.* **2002,** *124*, 1031−1039.

40. Dylla, A. G.; Janzen, D. E.; Pomije, M. K.; Mann, K. R., *Organometallics* **2007,** *26*, 6243-6247.

41. Sun, Y.; Ye, K.; Zhang, H.; Zhang, J.; Zhao, L.; Li, B.; Yang, G.; Yang, B.; Wang, Y.; Lai, S. W.; Che, C. M., *Angew. Chem., Int. Ed.* **2006,** *45*, 5610-5613.

42. Díez, A.; Fornies, J.; Larraz, C.; Lalinde, E.; López, J. A.; Martin, A.; Moreno, M. T.; Sicilia, V., *Inorg. Chem.* **2010,** *49*, 3239-3251.

43. Holland, L.; Shen, W.-Z.; von Grebe, P.; Sanz Miguel, P. J.; Pichierri, F.; Springer, A.; Schalley, C. A.; Lippert, B., *Dalton Trans.* **2011,** *40*, 5159-5161.

44. Bondi, A., *J. Phys. Chem.* **1964,** *68*, 441-451.

45. Connick, W. B.; Marsh, R. E.; Schaefer, W. P.; Gray, H. B., *Inorg. Chem.* **1997,** *36*, 913-922.

46. Charmant, J. P. H.; Forniés, J.; Gómez, J.; Lalinde, E.; Merino, R. I.; Moreno, M. T.; Orpen, A. G., *Organometallics* **1999,** *18*, 3353-3358.

47. Aullón, G.; Alvarez, S., *Chem. Eur. J.* **1997,** *3*, 655-664.

48. Haneder, S.; Da Como, E.; Feldmann, J.; Lupton, J. M.; Lennartz, C.; Erk, P.; Fuchs, E.; Molt, O.; Münster, I.; Schildknecht, C.; Wagenblast, G., *Adv. Mater.* **2008,** *20*, 3325-3330.

For table of contents use only

Pt_2Tl Building Blocks for 2D Extended Solids: Synthesis, Crystal Structures and Luminescence

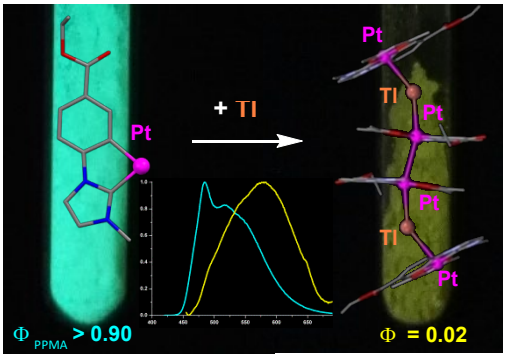

Synopsis

New *β*-diketonate compounds of Pt(II) containing several cyclometalated NHC ligands (R-C^C*) have been prepared and reacted with $TlPF_6$ to reach the Pt_2Tl clusters, $[\{Pt(R\text{-}C\hat{}C^*)(acac)\}_2Tl]PF_6$, held together by Pt-Tl bonds. The nature and position of the R substituents determine the efficiency of the emission and the ability of the clusters to self-assemble in 2D extended lattices through intermolecular interactions.